



ARTICLE

Progranulin deficiency confers resistance to autoimmune encephalomyelitis in mice

Katja Schmitz¹, Annett Wilken-Schmitz¹, Verica Vasic², Robert Brunkhorst³, Mirko Schmidt² and Irmgard Tegeder¹

Progranulin is a secreted neurotrophin that assists in the autophagolysosomal pathways that contribute to MHC-mediated antigen processing, pathogen removal, and autoimmunity. We showed that patients with multiple sclerosis (MS) have high levels of circulating progranulin and that its depletion in a mouse model by a monoclonal antibody aggravates MS-like experimental autoimmune encephalomyelitis (EAE). However, unexpectedly, progranulin-deficient mice ($Grn^{-/-}$) were resistant to EAE, and this resistance was fully restored by wild-type bone marrow transplantation. FACS analyses revealed a loss of MHC-II-positive antigen-presenting cells in $Grn^{-/-}$ mice and a reduction in the number of CD8+ and CD4+ T-cells along with a strong increase in the number of scavenger receptor class B (CD36+) phagocytes, suggesting defects in antigen presentation along with a compensatory increase in phagocytosis. Indeed, bone marrow-derived dendritic cells from $Grn^{-/-}$ mice showed stronger uptake of antigens but failed to elicit antigen-specific T-cell proliferation. An increase in the number of CD36+ phagocytes was associated with increased local inflammation at the site of immunization, stronger stimulation-evoked morphological transformation of bone marrow-derived macrophages to phagocytes, an increase in the phagocytosis of *E. coli* particles and latex beads and defects in the clearance of the material. Hence, the outcomes in the EAE model reflect the dichotomy of progranulin-mediated immune silencing and autoimmune mechanisms of antigen recognition and presentation, and our results reveal a novel progranulin-dependent pathway in autoimmune encephalomyelitis.

Keywords: Progranulin; Autoimmunity; Antigen processing; Phagocytosis; Autoimmune encephalomyelitis

Cellular & Molecular Immunology (2020) 17:1077–1091; <https://doi.org/10.1038/s41423-019-0274-5>

INTRODUCTION

Progranulin is a secreted multifunctional neuroprotective and immunoregulatory protein. Loss-of-function mutations in humans are associated with ubiquitin-positive, tau-negative frontotemporal lobar degeneration (FTLD),^{1,2} neuronal lipofuscinosis,³ and other rare neurodegenerative diseases.⁴ Progranulin is constitutively expressed in the neurons of the central and peripheral nervous systems, activated immune cells of myeloid origin including macrophages and microglia, and oligodendrocytes in response to stress or brain trauma.^{5–7} Its deficiency in mice partly mimics the human disease and pathology of frontotemporal lobar degeneration.^{8,9} It is well accepted that neuroinflammation essentially contributes to neurodegeneration^{10,11} but whether progranulin produced within neurons and progranulin produced and released by immune cells are similarly protective in this respect is still debated. Although a number of receptors, including Notch,¹² tumor necrosis factor alpha (TNF α),¹³ and Ephrin 2A receptors,¹⁴ have been identified, current data suggest that progranulin also fulfils receptor-independent intracellular functions, which appear to converge on autophagolysosomal degradation pathways.^{15–18} Its complex interactions account for multifaceted effects in the CNS and in the periphery that are still incompletely understood. The peripheral effects include wound healing,¹⁹ a reduction in joint inflammation,¹³ the protection of the kidney against ischemia-

reperfusion injury²⁰ and the acceleration of tumor growth.²¹ The antagonism of TNFRs appears to be a logical explanation of its immune regulatory functions,¹³ but this is not without debate. TNF-independent mechanisms such as Notch- or EphR-mediated immune cell maturation and migration and the promotion of regulatory T-cells^{22,23} have only recently been recognized as putative alternative progranulin-sensitive pathways.

In contrast to the notion that progranulin acts as an immune silencer,¹¹ it also contributes to the clearance of pathogens, in particular *Listeria*^{8,17} and human immunodeficiency virus,²⁴ suggesting that progranulin fosters the functions of the innate immune system. Indeed, granulin peptides have been shown to assist in the recruitment of CpG oligonucleotides to toll-like receptor 9 (TLR9),²⁵ which is a sensor of cytosolic DNA and is critical for defense against viral pathogens. TLR9 encounters granulin peptides within endolysosomal compartments,²⁶ a meeting that appears to trigger TLR9 maturation and downstream signaling of innate immunity. Progranulin deficiency leads to the upregulation of innate immune genes, in particular complement factors.¹¹ Hence, targeting to and processing within lysosomal compartments is critical to understanding the immune functions of progranulin.

In addition to the sortilin-mediated uptake and sorting of progranulin, there may be a direct path from the ER to the

¹Institute of Clinical Pharmacology of the Medical Faculty, Goethe-University, Frankfurt (Main), Germany; ²Institute for Microscopic Anatomy and Neurobiology, University Medical Center of the Johannes Gutenberg University, Mainz, Germany and ³Department of Neurology, Goethe University Hospital, Frankfurt am Main, Germany
Correspondence: Irmgard Tegeder (tegeder@em.uni-frankfurt.de)

Received: 14 April 2019 Accepted: 2 August 2019

Published online: 29 August 2019

autophagolysosome, possibly through an interaction with prosaposin²⁷ or following the path of proteins destined for ER-associated degradation via autophagy²⁸ or the path of lysosomal enzymes. It has indeed been found to act as a lysosomal chaperone and recruit Hsp70 to lysosomal enzymes.^{18,29}

Autophagolysosomal mechanisms also essentially contribute to the processing of antigens and autoantigens and their presentation to class II major histocompatibility complex (MHC-II) and hence to the activation of the adaptive immune system.^{30,31} Dendritic cells (DCs) mainly capture antigens via MHC-II molecules at the cell surface, but some antigens gain access to MHC-II loading after macroautophagy, which serves as a constant antigen delivery machinery for MHC-II compartments³² and essentially contributes to the response to some autoantigens.^{33,34} During this so-called endosome-mediated autophagy,³¹ MHC-II-containing endosomes are destined for autophagy via ubiquitin labeling and an interaction with the autophagy cargo receptor SQSTM1/p62, a process that is facilitated by progranulin.¹⁵

Considering the dual roles of autophagy in pathogen removal and autoimmunity and the previously observed proautophagic functions of progranulin, we hypothesized that the opposing pro- and anti-inflammatory and the neuroprotective effects of progranulin are critical for the development and progression of autoimmune dependent neuroinflammatory diseases. To address this question, we studied the effects of progranulin deficiency and overexpression in the experimental autoimmune encephalomyelitis (EAE) model of multiple sclerosis (MS) *in vivo* and the responses of immune cells from this model to antigens and pathogens *ex vivo*. We showed that progranulin deficiency leads to EAE resistance due to enhanced phagocytosis and the failure of antigen processing or presentation.

RESULTS

High progranulin serum concentrations in patients with MS
Low progranulin serum and plasma levels are predictive of the progranulin mutation status in mutation carriers,³⁵ and high levels have been associated with inflammatory diseases;^{36,37} the latter may be due to the activity or resolution of inflammation. In a cross-sectional cohort of patients with MS ($n = 102$; demographic data in Supplementary Table 1), progranulin serum concentrations were significantly higher in MS patients than in healthy controls ($n = 301$) (Fig. 1a; two-tailed, unpaired Student's *t*-test; $t = 5.273$, $df = 395$, $P < 0.0001$). There was no significant difference between the ICD10 subgroups (1st diagnosis, RRMS without relapse, RRMS acute relapse, PPMS, or SSMS), but RRMS patients with and without acute relapse showed the highest levels, which differed significantly from those of controls (one-way ANOVA; $F(4,392) = 9.217$, $P < 0.0001$; Sidak post hoc test; healthy vs. RRMS no relapse, $P < 0.001$; RRMS with acute relapse, $P < 0.0001$). Linear regression analysis did not show a significant relationship between progranulin serum levels and expanded disability status scale (EDSS) score ($P = 0.1704$) (Supplementary Fig. 1) or the number of years since diagnosis (Supplementary Fig. 1). Progranulin serum levels were positively associated with high levels of C16 ceramide, which has been shown to be elevated in MS patients³⁸ and in EAE models³⁹ (Supplementary Fig. 1). Long-term follow-up studies of individual patients revealed fluctuations in progranulin levels in association with disease activity (Supplementary Fig. 1e), which is in agreement with previous studies that showed high progranulin CSF levels in patients with radiologically isolated syndrome⁴⁰ and neuromyelitis optica.⁴¹

Progranulin deficiency confers EAE resistance

To address the functional role of progranulin in the context of MS, we employed the EAE model in mice.

Out of 16 $Grn^{-/-}$ mice, only 3 developed very mild EAE symptoms (score 0.5), whereas all 16 controls developed typical EAE. The EAE incidence differed significantly between the groups ($P > 0.0001$). Accordingly, the clinical EAE scores of $Grn^{-/-}$ mice were much lower than the scores of the controls, and there was no EAE-evoked weight loss in $Grn^{-/-}$ mice (Fig. 1b). Notably, $Grn^{-/-}$ mice were "overweight" at baseline and throughout the experiment, which is in agreement with previous observations.⁴² As expected from the clinical course, almost no immune cells infiltrated the spinal cord or the brain in $Grn^{-/-}$ mice, as demonstrated by immunofluorescent studies of Iba1-positive cells (Fig. 1c–e) and FACS analyses of CD45 + CD11b + macrophages or microglia and CD45 + MHC-II + antigen-presenting cells (Fig. 1f). The sample sizes and statistics are shown in Fig. 1.

BMX restores EAE susceptibility in $Grn^{-/-}$ mice

The transplantation of bone marrow from either LysM- Grn -OE progranulin-overexpressing mice or from wild-type donors into irradiated $Grn^{-/-}$ mice restored EAE susceptibility in $Grn^{-/-}$ mice; the mice showed normal clinical EAE scores and normal EAE-evoked weight loss (Fig. 2a, b). The overexpression of progranulin in myeloid cells per se did not affect the EAE course. Both the EAE incidence and clinical scores of LysM- Grn -OE mice did not differ from those of floxed control mice (Fig. 2c), but weight loss was mildly reduced (2-way ANOVA for group; $F(1,323) = 3.888$; $P = 0.0495$). This was accompanied by a lower number of T-cells in the spinal cord (Fig. 2c). Hence, in disagreement with the knockout data, progranulin overexpression in myeloid cells was mildly protective. To address this inconsistency, we depleted progranulin (presumably mostly extracellular progranulin) with a monoclonal anti-PGRN antibody (Fig. 2d), and this treatment resulted in the aggravation of clinical EAE scores (Fig. 2e). The results suggested that progranulin has antiinflammatory effects but is also required for the initiation of the autoimmune response, which involves the uptake, processing and presentation of the myelin oligodendrocyte glycoprotein (MOG) antigen, which fostered by the adjuvant effect of heat-inactivated mycobacteria (CFA). *In vivo* imaging of the site of immunization in $Grn^{-/-}$ mice and controls (Fig. 2f) revealed more local inflammation, suggesting more phagocyte infiltration in response to CFA and possibly stronger phagocytotic activity, as suggested by previous studies.⁴³ Hence, EAE resistance in $Grn^{-/-}$ mice likely reflects an inherent defect in the initiation of EAE.

Shift of myeloid cell populations in $Grn^{-/-}$ mice: the loss of MHC-II + APCs and an increase in the number of scavenger receptor class B phagocytes

To understand the underlying mechanisms, we performed FACS analyses of immune cell populations and cytokines from the spleen, the peripheral blood and the site of immunization. Forward scatter (FSC) vs. side scatter (SSC) plots showed a relative increase in the number of small mononuclear cells, which are likely naive, nonprimed lymphocytes, in $Grn^{-/-}$ mice (Fig. 3a). This assumption was based on the subsequent gating of mononuclear cells for MHC-II and CD36 (Fig. 3b). The scatter plots and histograms revealed a complete loss of MHC-II + antigen-presenting cells in $Grn^{-/-}$ mice but a strong increase in the number of CD36+ cells (Fig. 3b, c). Both effects occurred independent of EAE; they were also evident in control mice that received CFA without the MOG35-55 peptide. $Grn^{-/-}$ cells from EAE mice (mice that were immunized but did not show EAE symptoms) adopted a polymorphic morphology (SSC-high) and produced high amounts of IFN γ and IL-10 upon restimulation *ex vivo* (Fig. 3d). In contrast, there was no EAE-evoked proliferation of CD11b+ myeloid cells in the spleen of $Grn^{-/-}$ mice (Fig. 3e), reflecting differences in disease activity. CD11b+ cells constitute the major group of myeloid cells that invade the spinal cord in the EAE model (Fig. 1f).

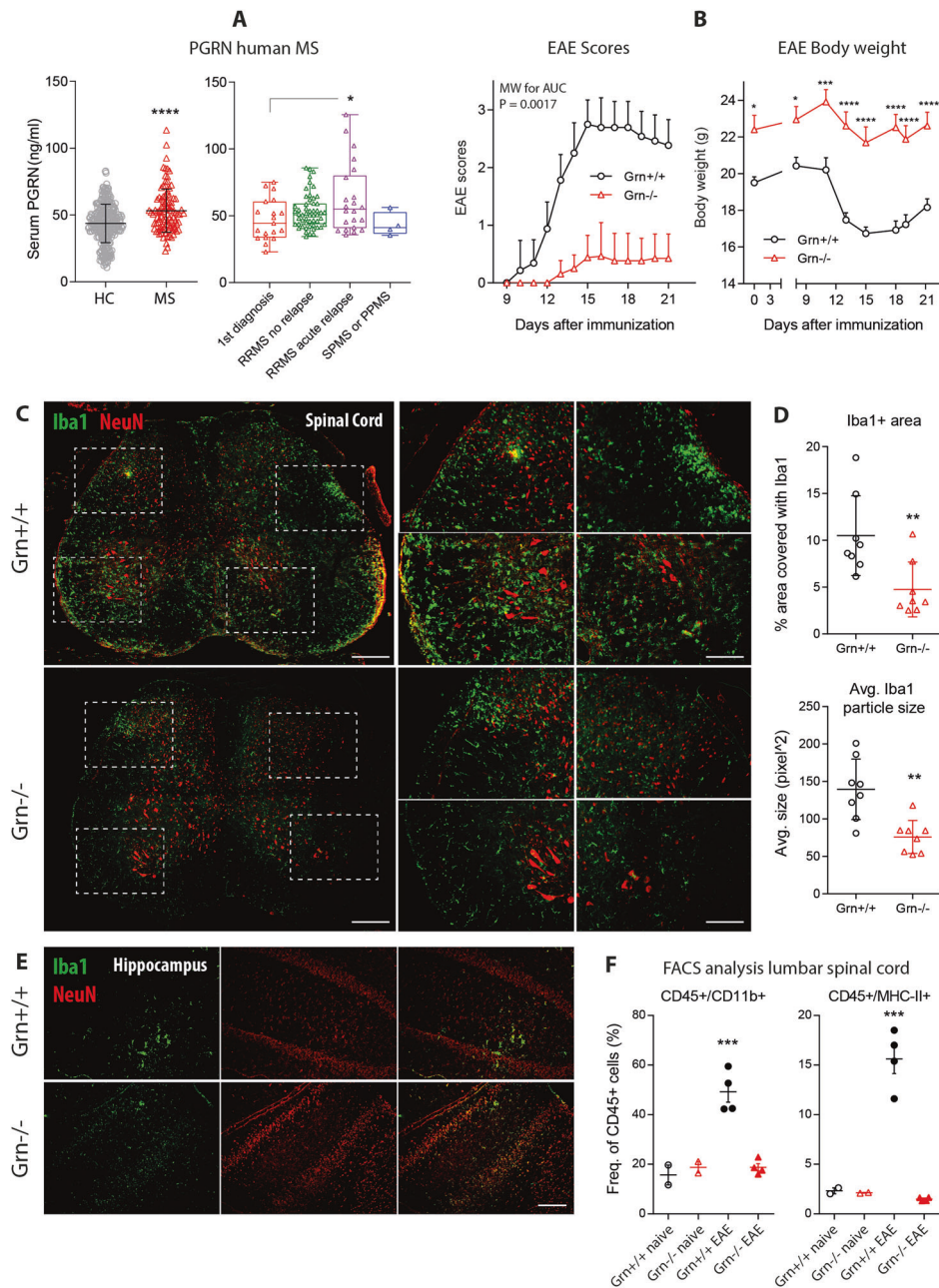


Fig. 1 Serum progranulin concentrations in MS patients and disease course in EAE in progranulin-deficient mice. **a** Scatter plots (mean with SD) and a box-scatter plot of progranulin serum concentrations in 102 patients with multiple sclerosis and 301 healthy controls. The box shows the interquartile range, the line is the median, and the whiskers show the minimum and maximum. The data were analyzed by two-sided unpaired Student's *t*-test for healthy vs. MS and one-way ANOVA followed by post hoc *t*-tests between each group using an adjustment of alpha according to Sidak for patient subgroups. The asterisks indicate significant differences between the groups; **P* < 0.05, *****P* < 0.0001. RRMS, relapsing-remitting MS; SPMS, secondary progressive MS; PPMS, primary progressive MS. **b** Time courses of the clinical EAE scores (mean ± 95% CI) and body weights (mean ± SEM) of Grn^{+/+} versus Grn^{-/-} mice in MOG-induced primary progressive EAE. The AUCs of the scores were compared with the Mann–Whitney U test. The time courses of the body weights were analyzed using 2-way ANOVA and subsequent *t*-tests for each time point using an adjustment of alpha according to Sidak. The asterisks indicate significant differences between groups; *n* = 16 per group; **P* < 0.05, ****P* < 0.001, *****P* < 0.0001. **c** Representative immunofluorescence images of the myeloid marker Iba1 in the lumbar spinal cord of Grn^{+/+} and Grn^{-/-} mice 21 days after EAE induction. NeuN was used to counterstain the neurons. The right panel shows higher magnification images of the indicated regions. Scale bar = 200 μm for overviews and 50 μm for high-magnification images. **d** Scatter plots showing the quantification of the Iba1+ area and the average size of Iba1+ particles in the lumbar spinal cord of Grn^{+/+} and Grn^{-/-} mice 21 days after EAE induction. The scatter shows the analysis of images of stitched SC sections at different sites (*n* = 3 mice per group with 2–3 images per mouse). Each full spinal cord section is made of 10–12 tiled images. The line is the mean, and the whisker shows the SD. The data were analyzed by unpaired two-sided Student's *t*-test. The asterisks indicate significant differences between the groups; ***P* < 0.01. **e** Representative Iba1 immunofluorescence of the hippocampus of Grn^{+/+} and Grn^{-/-} mice 21 days after EAE induction. NeuN was used to counterstain the neurons. *n* = 3 per group. Scale bar = 50 μm. **f** FACS analysis of the lumbar spinal cord from naive mice and EAE Grn^{+/+} and Grn^{-/-} mice 21 days after EAE induction. Each dot represents one mouse. The scatter shows the number of CD45 + CD11b + myeloid cells, which represent microglia and macrophages, and of CD45 + MHC-II + leukocytes, which represent antigen-presenting cells (APCs). The data from the EAE mice were compared with two-tailed unpaired *t*-tests. The asterisks indicate significant differences between the groups; ****P* < 0.001

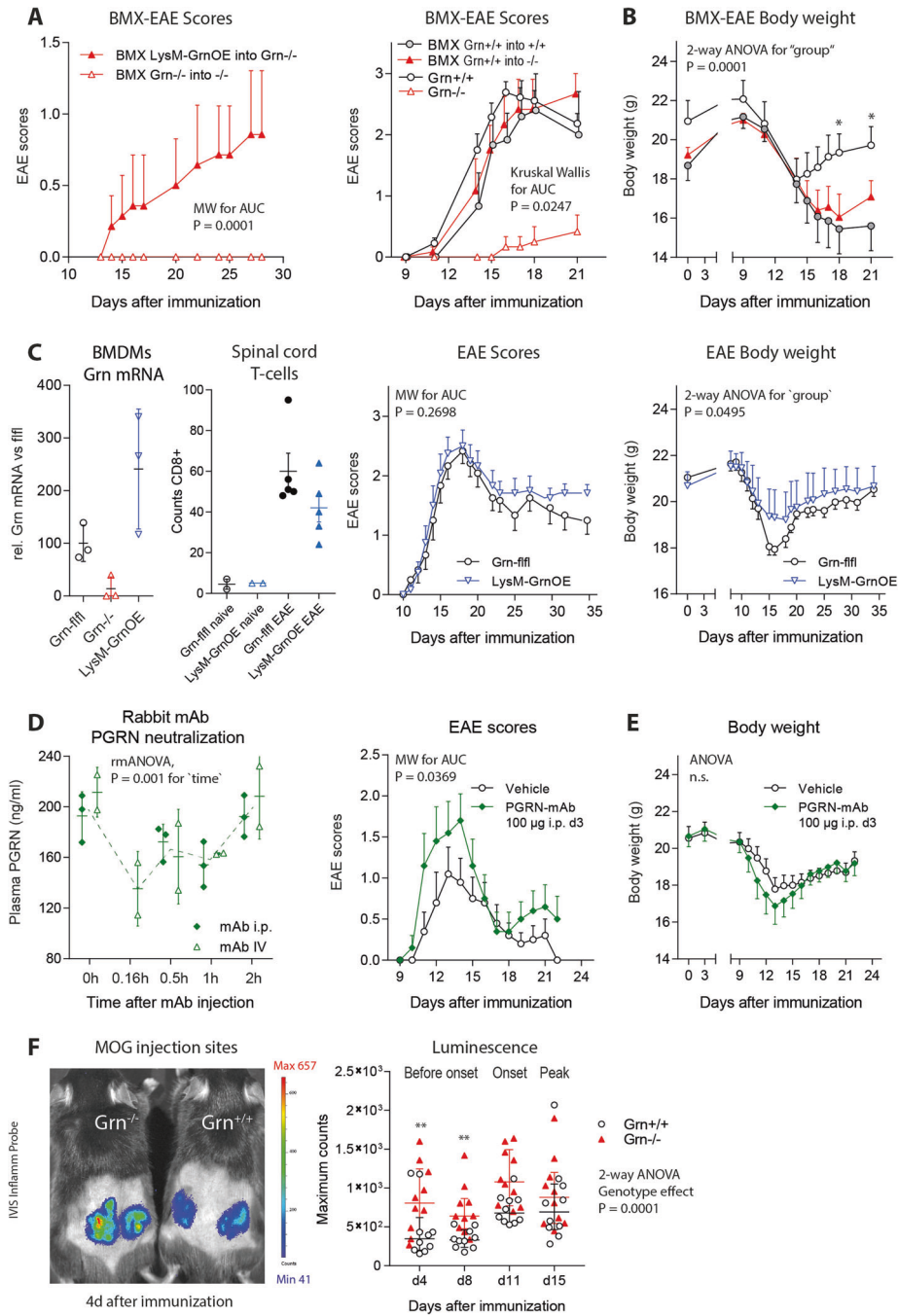


Fig. 2 Rescue of EAE susceptibility in progranulin-deficient mice upon transplantation with wild-type bone marrow. **a** Time courses of the EAE scores of Grn^{-/-} mice after bone marrow transplantation (BMX) from LysM-GrnOE or Grn^{-/-} mice (mean ± SEM). BMX was performed 3 weeks before EAE induction. LysM-GrnOE mice overexpress progranulin specifically in myeloid cells. The AUCs of the scores were compared with the Mann-Whitney U test; *n* = 8 per group. **b** Time courses of the EAE scores and body weights of Grn^{+/+} and Grn^{-/-} mice with and without BMX of Grn^{+/+} bone marrow (mean ± SEM). The AUCs of the scores were compared with the Kruskal Wallis test, and body weights were compared with 2-way ANOVA followed by post hoc analysis for each time point using a correction of alpha according to Sidak. The asterisks indicate significant differences between the groups; *n* = 9 Grn^{+/+} and *n* = 10 Grn^{-/-}; **P* < 0.05. **c** Relative mRNA levels of progranulin in bone marrow-derived macrophages from Grn^{fl/fl}, Grn^{-/-} and LysM-GrnOE mice confirming overexpression, the number of T-cells infiltrating the spinal cord and time courses of EAE scores and body weights of Grn^{fl/fl} and LysM-GrnOE mice (*n* = 10 for EAE). The statistical analyses were the same as those used in **b**. **d** Neutralization of plasma progranulin upon intraperitoneal or intravenous injection of monoclonal progranulin antibody (PGRN mAb) in three mice per group. Plasma progranulin concentrations were analyzed by ELISA up to 2 h after mAb injection. For statistics, i.p. and IV injection data were summarized and analyzed by 2-way ANOVA with time as the factor. **e** Time courses of EAE scores and body weights (mean ± SEM) of C57Bl/6 mice treated with vehicle or progranulin antibody (100 µg PGRN mAb administered i.p. 3 days after immunization). The statistical analyses were the same as those used in **b**. *n* = 16 per group. PGRN mAb significantly aggravated the EAE course. **f** In vivo luminescence imaging of local skin inflammation at the MOG/CFA injection sites using a bioluminescent inflammation probe. The scatter plots show the quantification of the maximum counts in the regions of interest of *n* = 6 mice per group at the two maximum time points of each animal. Images were captured 5 and 10 min after probe injection. The counter were log₁₀ transformed and analyzed by 2-way ANOVA with factors of time and genotype followed by post hoc analysis of each time point using an adjustment of alpha according to Sidak. The asterisks indicate significant differences between the groups; ***P* < 0.01

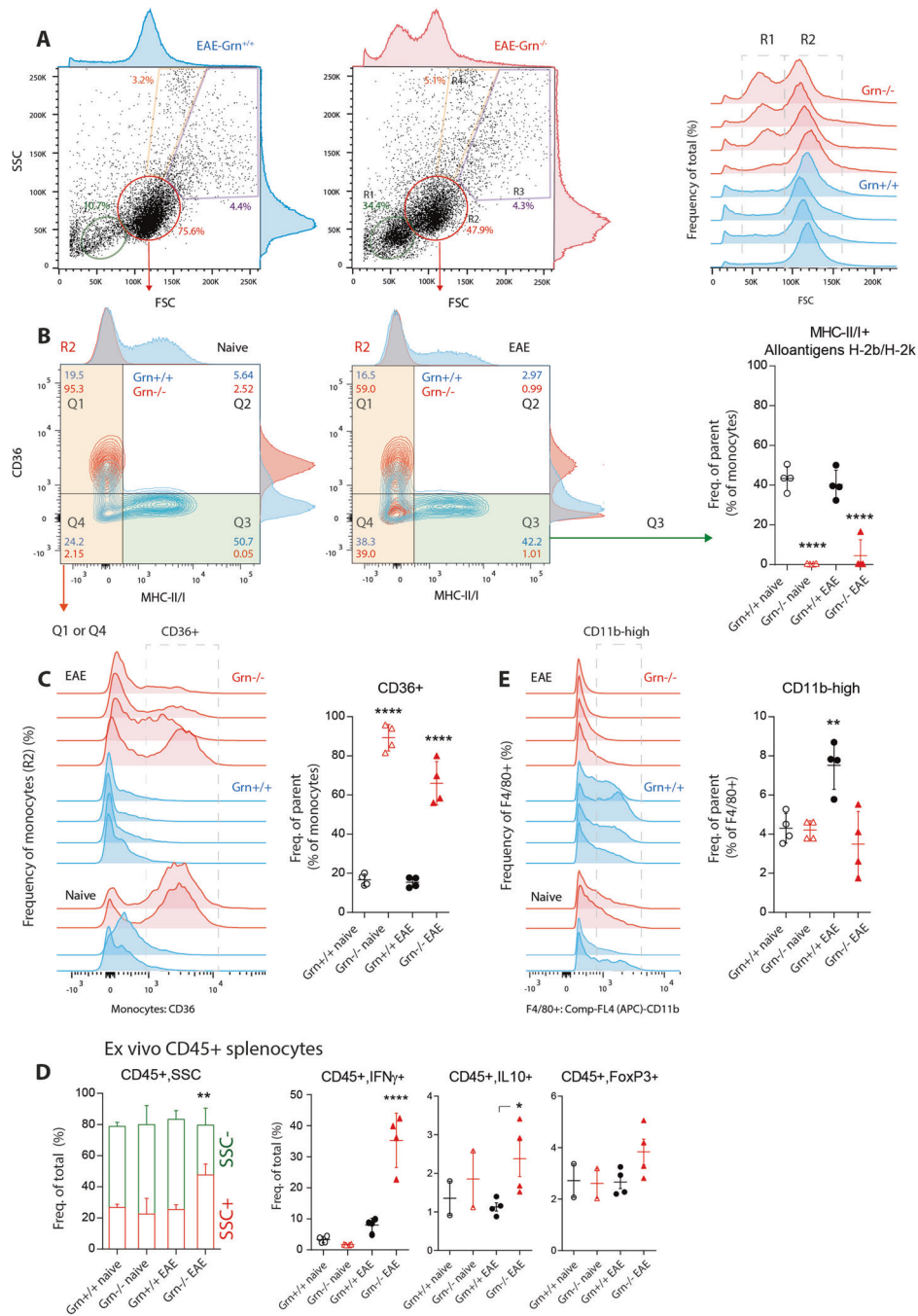


Fig. 3 FACS analysis of splenic myeloid cell populations in EAE in progranulin-deficient mice. **a** Exemplary scatter plots and histograms showing FACS analyses of splenocyte subpopulations from $Grn^{+/+}$ and $Grn^{-/-}$ EAE mice 21 days after EAE immunization. Splenocytes were gated according to size (FSC, forward scatter) and granularity (SSC, side scatter). The green and red framed areas show lymphocytes (R1) and mononuclear cells (R2), which are represented as histograms in the right panel ($n = 4$ mice per group). **b** Representative contour plots and histograms of R2-mononuclear cells (red population in **a**) from naive mice and EAE $Grn^{+/+}$ and $Grn^{-/-}$ mice. Gated R2 cells were further gated for the expression of APC markers and the scavenger receptor CD36. Q3 shows MHC-II/I-positive APCs (alloantigens H-2A, H-2E, H-2K), and the right panel shows the quantification. The data were analyzed by one-way ANOVA, followed by post hoc analysis with adjustment of alpha according to Sidak. The asterisks indicate significant differences between the groups; $n = 4$ mice per group; $****P < 0.0001$. The Q1∩Q4 area shows MHCII-negative cells, which were further analyzed in **c**. **c** Histogram of mononuclear cells (gate R2 in panel **a**, gates Q1∩Q4 in **b**) analyzed for the expression of CD36, which is a scavenger class B receptor and marker of phagocytes. The indicated area highlights the CD36-positive cells used for quantification. The statistical analyses were the same as those used in **b**. The asterisks indicate significant differences between the groups; $****P < 0.0001$. **d** Stacked bars showing the number of granular leukocytes (SSC+ CD45+, red) and nongranular leukocytes (SSC- CD45+, green) in ex vivo cultures of splenic immunocytes from naive mice and EAE $Grn^{+/+}$ and $Grn^{-/-}$ mice and scatter plots of subpopulations of CD45+ cells in these cultures. Cells were restimulated with PMA/ionomycin ex vivo and, secretion was blocked with brefeldin A. The data were analyzed by 2-way ANOVA with population and group as factors followed by Sidak post hoc test of the groups or by one-way ANOVA followed by Sidak post hoc test. The asterisks show significant differences between $Grn^{+/+}$ and $Grn^{-/-}$ mice; $**P < 0.01$; $****P < 0.0001$. **e** Histogram of the analysis of CD11b expression in viable cells that were F4/80-positive splenic immunocytes and the quantification of cells expressing high levels of CD11b in the framed area. The statistical analyses were the same as those used in **b**; $**P < 0.01$

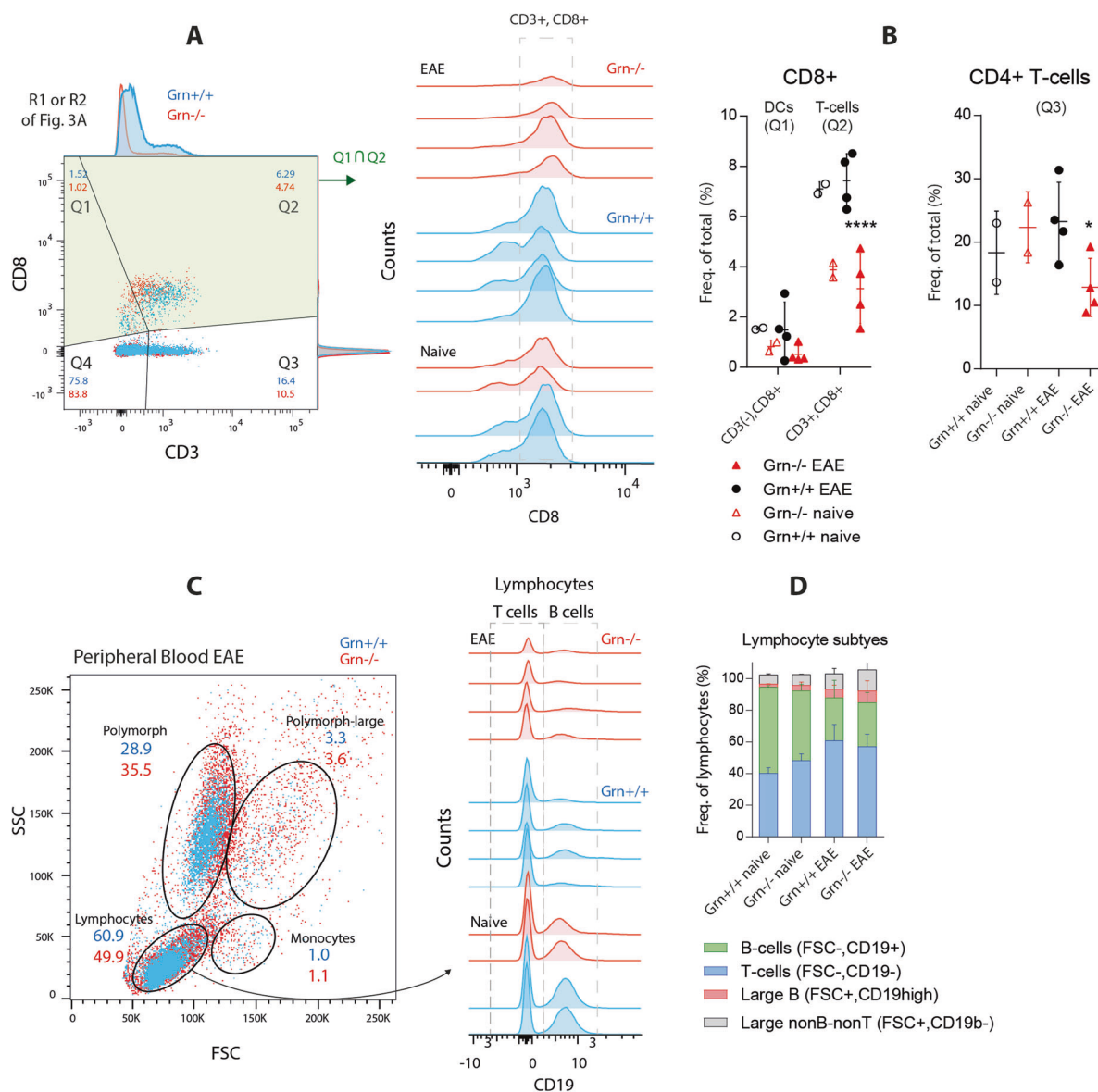


Fig. 4 FACS analysis of T cell populations in EAE in progranulin-deficient mice. **a** FACS analysis showing representative scatter dot plots of splenic lymphocytes and mononuclear cells (R1 and R2 in Fig. 3a) in $Grn^{+/+}$ and $Grn^{-/-}$ mice 21 days after the induction of EAE. Q1 and Q2 show $CD8^+$ cells, which were further quantified in 4b. **b** Histogram of cells from gates Q1:Q2 in **a** from two naive mice and four EAE mice per group analyzed for CD8 expression. The indicated area of cells shows $CD3^+ CD8^+$ T cells, which are quantified in the left scatter plot, which also shows the number of $CD8^+$ dendritic cells, and in the right scatter plot, which shows the number of $CD8^-$ T-cells. Q1, Q2, Q3 refer to the respective gates in **a**. The results of EAE mice were analyzed with 2-way ANOVA with population and genotype as the factors followed by post hoc analysis with adjustment of alpha according to Sidak. The asterisks show significant differences between the groups; * $P < 0.05$, **** $P < 0.0001$. **c** FSC versus SSC scatter plots of peripheral blood leukocytes showing the gating of leukocyte subpopulations in EAE $Grn^{+/+}$ and $Grn^{-/-}$ mice 21 days after immunization. $n = 4$ per EAE group, $n = 2$ naive mice. Lymphocytes were further analyzed in 4d. **d** Histogram of the expression of the B-cell marker CD19. The indicated areas show $CD19^-$ T-cells and $CD19^+$ B-cells. The stacked bar charts show the quantification of lymphocyte subpopulations based on size and CD19 expression. The subpopulations did not differ between genotypes

Relative reduction in the number of T-cells in $Grn^{-/-}$ mice
Analyses of lymphocyte subpopulations in the spleen showed an overall reduction in the number of $CD3^+$ T-cells in $Grn^{-/-}$ mice, specifically both $CD3^+ CD8^+$ T-cells and $CD3^+ CD4^+$ T-cells (Fig. 4a, b). The result is in agreement with the genotype-dependent loss of MHC-II + APCs and hence the failure of antigen-specific T-cell proliferation. There was also a reduction in the number of nonlymphoid $CD8^+$ cells, presumably $CD8^+$ DCs, which are known to contribute to scavenger receptor-dependent antigen cross-presentation. In agreement with the FACS data from the spleen, the number of circulating lymphocytes in peripheral

blood was lower in $Grn^{-/-}$ mice, while the number of polymorphic cells was increased (Fig. 4c). The relative numbers of B- and T-cells were similar in both genotypes, and the numbers shifted from $CD19^+$ B-cells to T-cells during EAE in both groups (Fig. 4d).

Increase in phagocytosis in $Grn^{-/-}$ DCs and BMDMs
FACS analyses of splenic cells suggested a defect in MHC-II-mediated antigen recognition, processing, or presentation but an increase in nonspecific $CD36$ -dependent scavenging in $Grn^{-/-}$ DCs and macrophages. To test this hypothesis, we assessed phagocytosis and endocytosis in $Grn^{-/-}$ and control DCs and

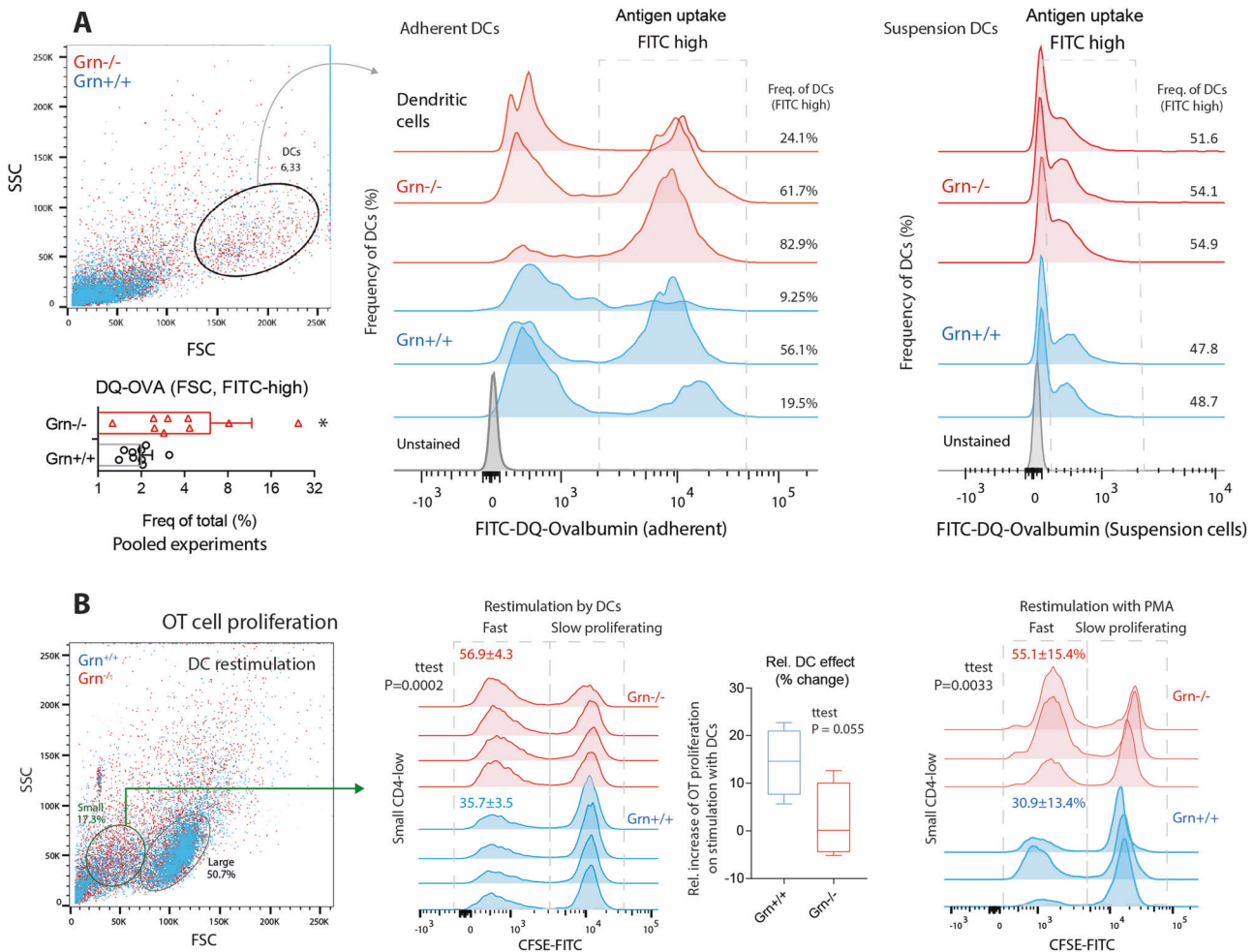


Fig. 5 Antigen uptake by primary dendritic cells and proliferation of T-cells in contact with sensitized DCs. **a** FACS analyses of Grn^{+/+} and Grn^{-/-} bone marrow-derived dendritic cells showing representative scatter dot plots and histograms of adherent (middle) and suspended (right) dendritic cells gated according to size (FSC) and granularity (SSC) and the uptake of ovalbumin-FITC. DC cultures were differentiated from myeloid bone marrow cells for 14 days and harvested 2 h after incubation with FITC-labeled DQ-ovalbumin (DQO). The framed areas in the histograms show FITC⁺ dendritic cells, which took up FITC-DQO. The scatter bar chart shows the quantification. Each dot represents one mouse. *n* = 8 Grn^{+/+}; *n* = 9 Grn^{-/-}. The data were analyzed by two-sided unpaired *t*-test. The asterisks show significant differences between the groups; **P* < 0.05). **b** FACS analyses of OT cell proliferation upon coculture with ovalbumin-stimulated dendritic cells or stimulation with PMA. OT cells were harvested from the spleen 4 days after ovalbumin injection, labeled with CFSE, and exposed to DCs or restimulated with PMA or vehicle. CFSE dilution indicates a high rate of proliferation. Grn^{-/-} OT cells show high proliferation (indicated by low CFSE) of small CD4^{low} nonantigen specific T-cells. The numbers are the means ± SD. Each scatter represents a culture from one mouse. *n* = 4 per group

bone marrow-derived macrophages (BMDMs). We used ovalbumin as an antigen and FITC-labeled *Escherichia coli* and latex beads for phagocytosis. CD36 accepts diverse protein and lipid ligands, likely including sulfatides from mycobacteria,^{44,45} and is involved in cell adhesion, phagocytosis, the metabolism of long-chain fatty acids,⁴⁶ and soluble CD5 ligand-stimulated autophagy.⁴⁷

Adherent and suspended Grn^{-/-} DCs showed an increased uptake of FITC- or PE-labeled ovalbumin (DQ-OVA) (Fig. 5a), showing that antigen recognition and internalization were enhanced. To assess whether the increase in antigen uptake was associated with antigen-specific T-cell proliferation, we used the CFSE carboxyfluorescein succinimidyl ester (CFSE) dilution technique. Indeed, the rate of proliferation of Grn^{-/-} T-cells was higher than the rate of proliferation of Grn^{+/+} T-cells (a higher fraction of CFSE-low cells), but this rapid proliferation was independent of stimulation with APCs (Fig. 5b); it was evident in the absence of stimulation. We inferred that the fast proliferating T-cells were not antigen specific and that there was no relative increase in the

proliferation of T-cells (compared to that of naive T-cells) evoked by sensitized Grn^{-/-} DCs (Fig. 5b, box plot). The results suggest that Grn^{-/-} DCs take up OVA but fail to elicit an antigen-specific T-cell response, pointing to defects in antigen digestion and presentation but not uptake.

As expected, the phagocytosis of pathogens was increased in Grn^{-/-} BMDMs with high CD36 levels, as determined by FITC-labeled *E. coli* (Fig. 6a) and IgG-FITC-labeled latex beads (Fig. 6b–e). The latter mimic IgG-opsonized pathogens and elicit complement activation, which is presumably overactive in progranulin knockout mice.¹¹ The exposure of BMDMs to the beads resulted in alterations in morphology towards phagocytes (FSC-high, SSC-high, Fig. 6b) and an increase in the number of CD11b^{high} cells (Fig. 6c, e), which did not occur in equally stimulated control cells. The increase in the expression of CD11b, which is part of the complement C3 receptor, is consistent with complement activation, and the morphologic switch toward large and polymorphic phagocytes is reminiscent of the stimulation of

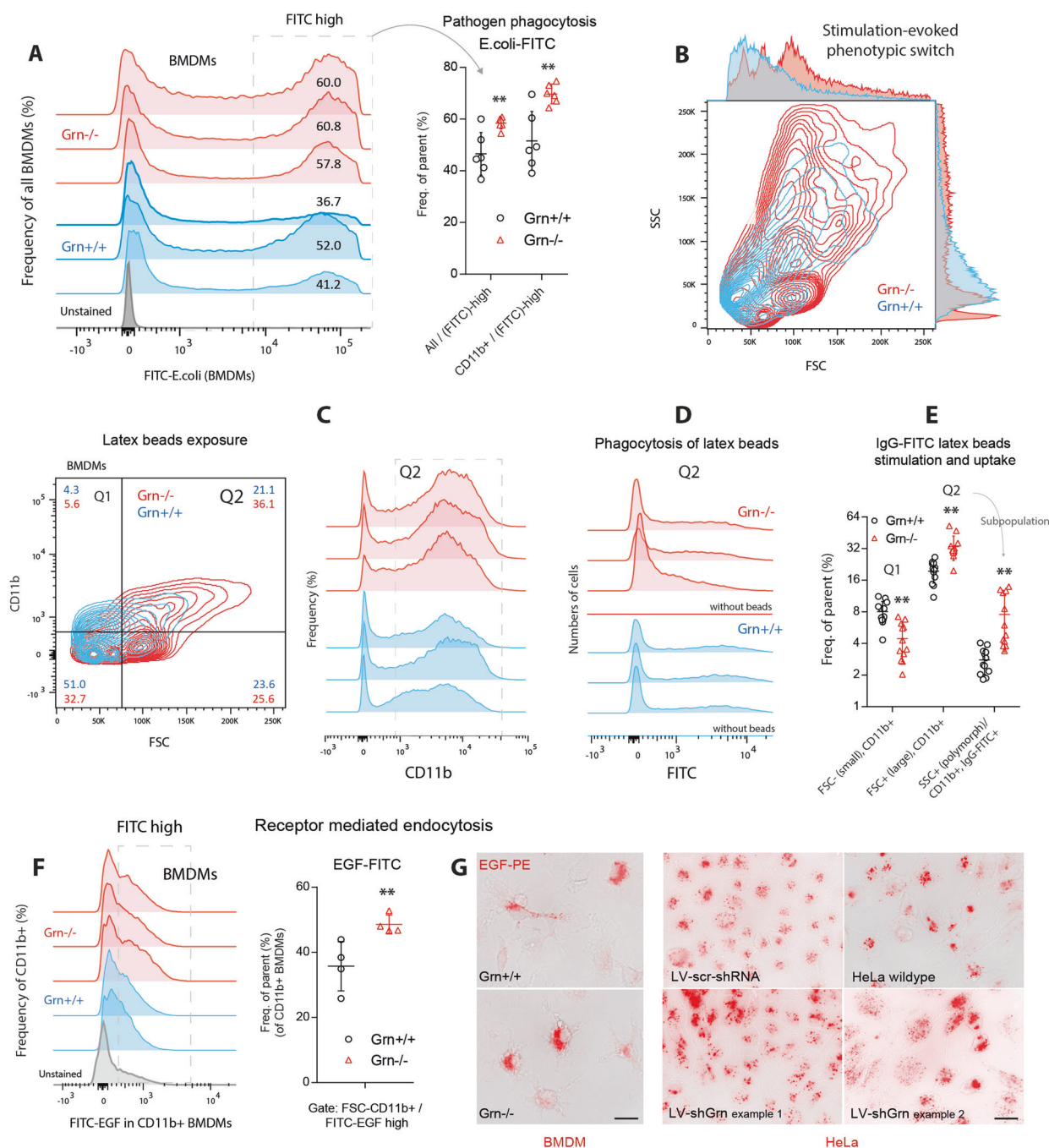


Fig. 6 Phagocytosis and receptor-mediated endocytosis of primary bone marrow-derived macrophages. **a** FACS analysis of bone marrow-derived macrophages (BMDMs) of three *Grn*^{+/+} and three *Grn*^{-/-} mice (two cultures per mouse) after stimulation with FITC-E. coli particles for 2 h. The framed area indicates FITC-positive BMDMs, which represent phagocytic cells. The scatter plots show the number of FITC+ cells. The data from each population were analyzed by two-sided unpaired *t*-test. The asterisks show significant differences between the groups; *******P* < 0.01. **b** Contour plots showing an example of the morphological transformation of BMDMs towards large polymorphic phagocytes upon exposure to IgG-FITC-labeled latex beads. Bone marrow stem cells were differentiated into BMDMs for 7 days and were treated with latex beads for 2 h. **c** Representative contour plots and histograms showing BMDMs gated according to size (FSC) and CD11b expression (quantification in **e**). **d** Histogram showing the number of FITC+ cells that phagocytosed FITC-IgG-labeled latex beads. **e** Number of CD11b^{low} and CD11b^{high} cells and FITC+ cells. Each scatter represents a culture from one mouse (*n* = 10 *Grn*^{+/+} mice and *n* = 11 *Grn*^{-/-} mice). The data were analyzed by 2-way ANOVA with population and genotype as factors followed by post hoc analyses according to Sidak. The asterisks show significant differences between the groups; *******P* < 0.01. **f** FACS analysis of EGFR-dependent endocytosis. Histograms and scatter plots showing the number of CD11b+ BMDMs in four *Grn*^{+/+} and *Grn*^{-/-} mice after exposure to FITC-labeled EGF particles. The framed area indicates the FITC-high population, which is quantified in the scatter plot. Each scatter represents a BMDM culture from one mouse. BMDMs were exposed to EGF-FITC for 30 min. The data were analyzed by unpaired two-sided Student's *t*-test. The asterisks show significant differences between the groups; *******P* < 0.01. **g** EGF-PE immunofluorescence images of BMDMs from *Grn*^{+/+} and *Grn*^{-/-} mice and of HeLa cells stably transduced with a lentiviral shRNA vector targeting progranulin¹⁵ (LV-shGrn) or scramble control vector (LV-scr-shRNA). The images show BMDMs and HeLa cells after 15 min of EGF-PE exposure. Scale bar = 10 μm

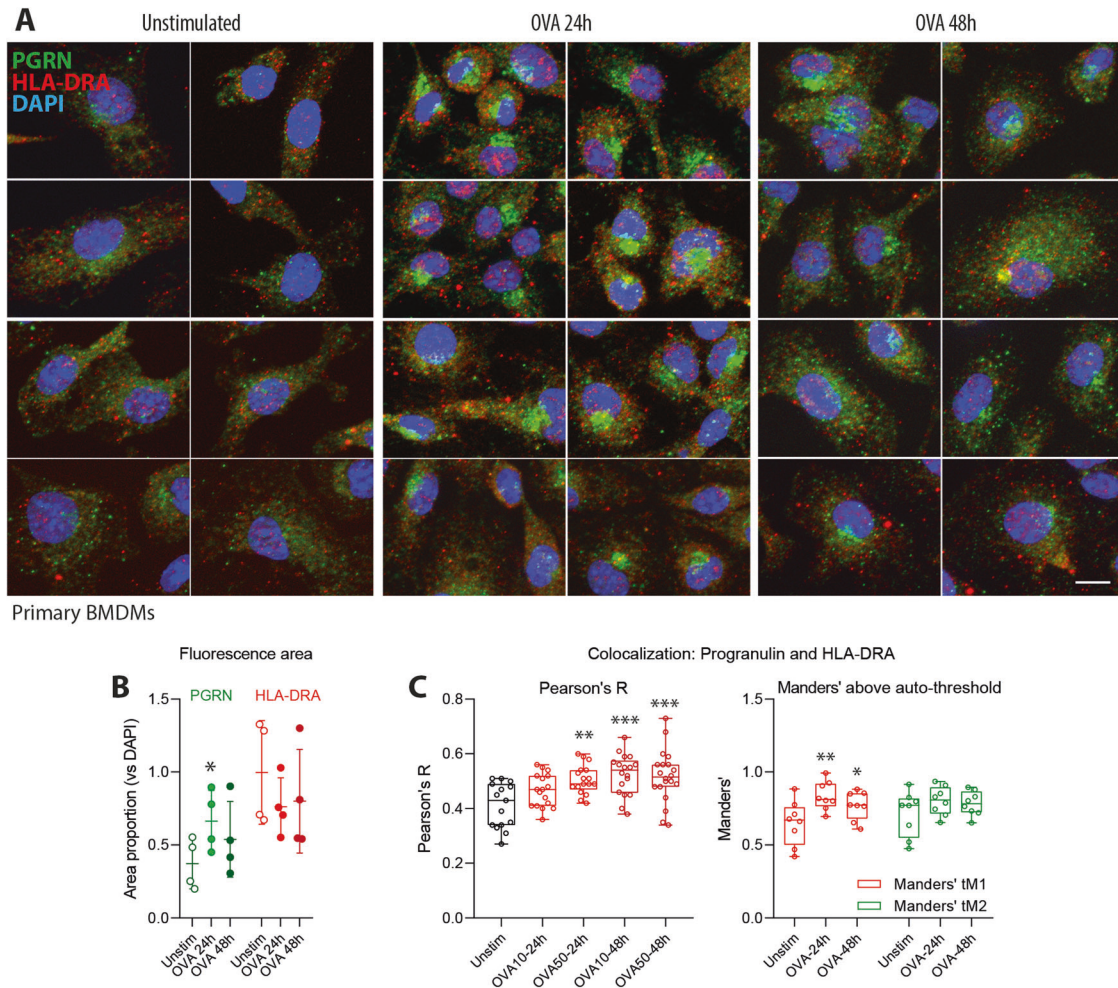


Fig. 7 Progranulin endocytosis and colocalization with HLA-DRA in ovalbumin-stimulated primary BMDMs. **a** Representative images of progranulin (green) and HLA-DRA (red) immunofluorescence in primary bone marrow-derived macrophages (BMDMs) with and without stimulation with 10 μ M ovalbumin for 24 or 48 h. DAPI was used as a nuclear counterstain (blue). Scale bar = 10 μ m. **b** The expression level of HLA-DRA and progranulin upon stimulation with OVA was assessed by analyzing the area of immunofluorescence after the threshold was set according to Li's algorithm in FIJI. The fluorescence areas were normalized to the DAPI area to account for the differences in the number of cells per image, and the areas were analyzed by two-way ANOVA followed by post hoc *t*-test with compared with unstimulated cells with a correction of alpha according to Dunnett. *n* = 4 cultures per condition. The line is the mean, and the whiskers show the SD. The asterisks show significant differences between the groups; **P* < 0.05. **c** Quantitative 3D colocalization of progranulin and HLA-DRA immunofluorescence in apotome image stacks of six independent cultures per OVA dose and time point and analysis of up to four regions of interest (ROI) per stack. Each scatter shows the result of one ROI. The box shows the interquartile range, the line is the median and the whiskers show the minimum and maximum. Colocalization was assessed with FIJI using the Pearson's correlation coefficient and Manders' tM1 and tM2 coefficients above the auto thresholds for channel 1 (HLA-DRA, red) and channel 2 (progranulin, red). The coefficients were analyzed by one-way ANOVA followed by post hoc *t*-test compared with unstimulated cells with a correction of alpha according to Dunnett. The asterisks show significant differences between the groups; **P* < 0.05, ***P* < 0.01, ****P* < 0.001

toll-like receptors. Overall, the phagocytosis of the beads was increased (Fig. 6d, e). Grn^{-/-} BMDMs also strongly endocytosed EGF-FITC (Fig. 6f), and similar results were obtained in Grn-knockdown HeLa cells (described in ref. ¹⁵; Fig. 6g), which strongly express EGFR and are a model of receptor-mediated endocytosis.

Hence, we infer that the 'appetite' of Grn^{-/-} BMDMs for antigens and pathogens is increased but is likely associated with the accumulation of the ingested material without proper elimination. The notion is consistent with previous studies that demonstrated a defect in autophagolysosomal processing.^{16–18,48} In support of this, upon lipopolysaccharide (LPS) stimulation of BMDMs, immunofluorescence showed an increase in the number of SQSTM1/p62-positive dots but a reduction in the size of LAMP1-positive lysosomes, suggesting an arrest of the autophagolysosomal flux (Supplementary Fig. 2), which is similar to previous observations in neurons.¹⁵

Progranulin endocytosis and colocalization with HLA-DRA in ovalbumin-stimulated BMDMs

To further address the underlying mechanisms of the observed antigen processing/presentation defects in the absence of progranulin, we assessed the pathways of progranulin and its colocalization with the MHC-II HLA-DRA molecule in BMDMs stimulated with ovalbumin (Fig. 7a–c). HLA-DRA was chosen because a previous yeast-2-hybrid study that used progranulin as bait identified HLA-DRA as a putative interaction partner of progranulin.^{15,49} In unstimulated cells, progranulin-positive dots were distributed throughout the cytoplasm with a subtle predilection of perinuclear sites (Fig. 7a). However, upon OVA stimulation, the immunoreactivity of progranulin strongly increased (Fig. 7a, b), suggesting that it was endocytosed, and progranulin accumulated in perinuclear vesicle heaps (Fig. 7a), likely representing autophagolysosomes. This accumulation was

strongest at 24 h and then partially resolved. At baseline, the progranulin-positive dots and HLA-DRA-positive dots were segregated (Fig. 7a, c), but colocalization increased upon OVA stimulation, suggesting that progranulin was endocytosed along with HLA-DRA and the antigen or that vesicles fused upon vesicle maturation.

DISCUSSION

We showed that progranulin serum levels are increased in patients with RRMS and that progranulin-deficient mice are resistant to immunization-evoked EAE even though progranulin is supposed to inhibit inflammatory processes. At first, this appears to be an inconsistency. Indeed, high levels of circulating progranulin in the plasma or CSF are associated with the progression of Alzheimer's disease,⁵⁰ neuromyelitis optica,⁴¹ autoimmune arthritis,³⁷ and insulin resistance.⁵¹ However, a deficiency in progranulin causes neuroinflammation^{8,11,52} and is associated with a high prevalence of some autoimmune diseases,⁵³ and progranulin autoantibodies sustain a proinflammatory environment.⁵⁴ In contrast, recombinant progranulin limits damage in models of brain ischemia and trauma^{6,55} and promotes the maturation of regulatory anti-inflammatory T-cells.^{22,23} The observed association between PGRN and RRMS does not demonstrate causality. Progranulin may be proinflammatory or proresolving, and the initiation of autoimmunity and the maintenance of inflammation are differently affected by lysosomal processing.

Our data showed that progranulin is required for autoantigen processing and presentation and is hence particularly relevant for the autoimmune-driven initiation of inflammatory processes. The transplantation of wild-type bone marrow restored EAE susceptibility in *Grn*^{-/-} mice, showing that the defect originates in myeloid cells, including antigen-presenting cells, rather than T-cells, which proliferate faster but not in an antigen-specific manner. The proportion of myeloid cells that express MHC-II on the cell surface was strongly reduced in progranulin-deficient mice, whereas antigen uptake by primary DCs or macrophages was increased, showing that the defect occurs downstream of endocytosis and during antigen processing or presentation.

Based on previous studies showing that progranulin assists with specific forms of autophagy¹⁵ and xenophagy¹⁷ by promoting the removal of protein aggregates or pathogens, we hypothesize that resistance to EAE is caused by alterations in antigen processing via autophagolysosomes. These vesicles crucially contribute to the processing of intracellular and extracellular antigens^{30,32} and regularly supply processed antigens to MHC-loading compartments.³² A recent study showed that noncanonical autophagy protein 5 (ATG5)-dependent phagocytosis contributes to the processing of myelin antigen and pathology in the EAE model.⁵⁶ Notably, DC-specific ATG5-deficient mice are resistant to adoptive transfer EAE; the resistance is not identical to but rather downstream of the *Grn*^{-/-} phenotype described here, and the mice have resistance to immunization-evoked EAE. Nevertheless, based on our previous studies that showed that progranulin binds to the ATG5-partner ATG12,¹⁵ there is some rationale that ATG5-dependent and progranulin-dependent antigen processing may converge on a common path. Indeed, ATG5-deficient DCs fail to present a myelin peptide to CD4⁺ T cells, although they normally phagocytose material from damaged oligodendrocytes.⁵⁶ In this context, it is also important to note that progranulin has been shown to stimulate the maturation or function of cathepsins,²⁹ which are crucial proteases involved in the processing of ovalbumin and myelin antigens.⁵⁷

Specifically, in DCs, the autophagolysosomal degradation pathway is activated upon endocytosis, and the resulting compartments harbor both autophagosomal markers and the molecular machinery for antigen processing.³¹ We observed previously in yeast-2-hybrid screens that progranulin interacts with HLA-DRA,⁴⁹

an essential component of MHC-II complexes. Here, we found the colocalization of progranulin and MHC-II in perinuclear vesicle-like structures upon OVA stimulation, suggesting a fusion of the vesicles or coendocytosis. Our FACS analyses show a striking decrease in the number of MHC-II-positive myeloid cells in progranulin knockout mice. We therefore suggest that progranulin assists in the autophagy-mediated processing of certain antigens, which is supported by a recent study showing that progranulin knockouts show defective xenophagy, which is an autophagy-related process, of *Listeria* pathogens.¹⁷ In addition, it was previously shown that the development of EAE is abrogated by the inhibition of autophagolysosomal flux,³³ strongly suggesting that myelin autoantigens are processed via this process.

Macroautophagy- and chaperone-mediated autophagy were initially mainly believed to deliver intracellular cytosolic antigens to MHC class II loading compartments,^{30,32} but it is now well accepted that autophagolysosomal processing also contributes to the delivery of extracellular antigens and pathogens and likely contributes to the pathophysiology of autoimmune neuritis.⁵⁸

The immune system of progranulin-deficient mice apparently adopts a number of compensatory mechanisms to address defects in adaptive immunity. For example, we observed a strong increase in the proportion of CD36 scavenger receptor-positive myeloid cells, an increase in receptor-mediated endocytosis and phagocytosis of *E. coli* particles and latex beads, stronger phenotypic transformation towards phagocytes upon treatment with latex beads or stimulation with LPS, and stronger nonspecific proliferation of T-cells upon exposure to phorbol 12-myristate 13-acetate (PMA). The defect in autophagolysosomal processing and the increase in CD36-mediated phagocytosis may reduce the adjuvanticity of mycobacteria, the processing of which partially depends on ubiquitin-dependent autophagy involving SQSTM1/p62 and ATG5⁵⁹ and scavenger receptor-mediated uptake.^{44,45}

The observed stronger phagocytic activity and the overactivation of innate immune responses explains the strong local inflammation at the site of immunization in progranulin knockout mice. The results are consistent with those of multiple previous studies showing that inflammation in the periphery and neuroinflammation in the brain are intensified in progranulin-deficient mice. This has been shown in models of arthritis,¹³ wound healing,¹⁹ brain trauma,⁵⁵ ischemia,⁶⁰ aging,¹¹ and neurodegenerative diseases.⁸ Hence, progranulin mostly inhibits inflammatory processes and promotes resolution. Mechanistically, the inhibition of TNF α receptors has been proposed as a major mechanism,¹³ but this is debated.⁶¹ In agreement with the proposed protective effects, we showed that the monoclonal antibody-mediated depletion of progranulin aggravates EAE in wild-type mice. Considering that the antibodies likely mainly neutralize secreted extracellular progranulin, we hypothesize that this protective effect relies on receptor signaling, with progranulin acting via extracellular receptor binding sites. The receptor-mediated process may involve one or more of the previously identified receptors, including the TNF α receptor,¹³ ephrin 2A receptors,¹⁴ and Notch.¹² It is of note that sortilin-deficient mice, i.e., mice that lack the progranulin reuptake transporter, do not exhibit EAE resistance upon progranulin knockout.⁶² Indeed, they are indistinguishable from their wild-type controls upon the induction of EAE.⁶² Hence, neither the proautoimmunity mechanisms of progranulin nor its antiinflammatory effects depend on sortilin-mediated reuptake in this model, strongly suggesting that progranulin follows a direct path towards autophagolysosomes and MHC-loading compartments.

We infer that the participation of progranulin in autophagy and related processes such as xenophagy¹⁷ and the participation of progranulin in antigen processing require sortilin-independent endocytosis or intracellular pathways that are independent of sortilin-mediated cycling^{63,64} and possibly involve direct transport from the ER to the autophagolysosome. The presence of

progranulin in the lysosome appears to enhance some proteolytic lysosomal functions,^{16,26} but the exact mechanisms are still elusive. Indeed, it has been suggested that progranulin acts as a lysosomal chaperone.^{18,65} Proteome analyses have revealed alterations in lysosomal protein profiles in microglia/macrophages in Grn^{-/-} mice, but the functional implications are unclear.¹⁷ Approximately equal numbers of lysosomal proteins, including enzymes, and lysosomal membrane proteins, are up- and down-regulated.¹⁷ Our previous Y2H studies demonstrated an interaction between progranulin and lysosomal-associated transmembrane protein 5,⁴⁹ which may be a cue for further research considering the association of lysosomal-associated transmembrane protein 5 with autoimmune diseases.⁶⁶ Irrespective of the mechanistic uncertainty, the functions of progranulin in the lysosome have an obvious immune-relevant impact, in particular on the processing of TLR9,²⁵ the degradation of *Listeria* antigen^{8,17} and possibly mycobacteria, and the processing of autoantigens, as suggested by the results of the present study.

Subsets of our patients with relapsing-remitting MS exhibited increased serum levels of progranulin, reflecting the activation of the immune system, which is consistent with the results of previous studies showing that the CSF levels of progranulin are associated with the course of MS^{40,67} and the progression of Alzheimer's disease.⁵⁰ Considering the dual roles of progranulin in promoting autoantigen processing and inhibiting inflammatory processes, including complement activation in the brain¹¹ and TNF α -mediated effects,¹³ the effects of high progranulin serum levels per se is equivocal. Individual time courses and comparisons of pre-post medication levels of the few patients in our study suggest that increase in the serum levels of progranulin coincide with relapses but that particularly low levels are associated with serious disease courses, refractory relapses, or glucocorticoid medication. Further time course observations in larger cohorts may provide further insight into the functions of progranulin in the context of human MS.

In summary, we showed that progranulin deficiency confers resistance to EAE in mice by impairing antigen processing and presentation but increasing antigen uptake. In combination with the results of previous studies, the data suggest that the autophagolysosomal processing of the myelin autoantigen and hence the development of MS autoimmunity involves the role of progranulin in the autophagolysosomal processing of autoantigens.

METHODS

Subjects and study design

The study followed the Declaration of Helsinki and was approved by the Ethics Committee of the Medical Faculty of the Goethe—University Frankfurt am Main, Germany. Informed written consent was obtained from all subjects. Employing a parallel group design, the study included patients with MS ($n = 102$, aged 18.2–62.8 years, 31 men) and healthy controls ($n = 301$, aged 18–53.2 years, 118 men). Outpatients and inpatients of the Department of Neurology (patients) and students and staff members of the hospital (controls) who routinely reported to the institutional occupational health service were consecutively recruited. The sample size was based on a previous study on lipid biomarkers in MS patients.⁶⁸ The collection of data and blood from MS patients was part of the local biobanking project (Neurological Department of the Goethe University, Frankfurt).⁶⁸ Inclusion criteria were age ≥ 18 years, a clinically verified diagnosis of MS based on ICD10 criteria (patients) or no current medical condition, as determined by a medical interview (controls), and no drug intake, except contraceptives, vitamins, and L-thyroxin, for at least 1 week. Demographic data, including time since diagnosis, EDSS scores and the current use of disease modifying medications, are summarized in Supplementary Tables 1 and 2.

Generation of progranulin-deficient and progranulin-overexpressing mice

Progranulin-expressing transgenic mice were used as previously described.¹⁵ A UbiC-driven loxP-flanked STOP cassette in front of mouse progranulin cDNA was inserted into the Rosa26 locus by homologous recombination. Mice were bred to homozygosity of the floxed allele (STOP-Grn^{fl/fl}). A PCR-based genotyping method was used to detect the wild-type allele (left: cgt gtt cgt gca agt tga gt and right: tgc gca tca caa gca ata at, 747 bp) and the floxed allele (left: gga tct gac atg gta agt aag c and right: gcc atc acc aca aga cac ac, 425 bp).

LysM progranulin-overexpressing mice were generated by mating LysozymeM-Cre mice with mice carrying the floxed STOP-Grn allele (STOP-Grn^{fl/fl}). LysoM-Cre-mediated recombination caused the deletion of the loxP-flanked STOP cassette in cells of the myeloid system, thereby leading to the UbiC-driven overexpression of progranulin in cells of myeloid origin, including macrophages, microglia, monocytes, and granulocytes.

Progranulin knockout mice (Grn^{-/-})⁸ were maintained in homozygous colonies. Sex- and age-matched C57BL/6J mice and STOP-Grn^{fl/fl} mice were used as controls, the latter in experiments involving Grn^{-/-} and OE animals. All mice were maintained on a C57BL/6J genetic background.

Animals and progranulin mAb treatment

Female SJL/J mice (10–12 weeks old) (Harlan Winkelmann, Germany) were used for relapsing-remitting EAE, and mice on a C57BL/6 background were used as models of primary progressive EAE. The mice were housed 3–5 mice per cage at constant room temperature (21 ± 1 °C) under a regular light/dark schedule with lights on from 7:00 a.m. to 7:00 p.m. Food and water were available *ad libitum*. Sample sizes followed the recommendations for EAE models (<https://hookelabs.com/protocols/>).

To neutralize progranulin, SJL/J-EAE mice were intraperitoneally (i.p.) administered 100 μ g of a progranulin monoclonal antibody (Sino Biological, # 50396-R034-50) 3 days after immunization. Control animals received vehicle. Neutralization efficacy was assessed by analyzing progranulin serum concentrations before and after antibody injection using a commercial ELISA kit (Adipogen, # AG-45A-0019-YEK-KI01).

The experiments were approved by the local Ethics Committee for Animal Research (Darmstadt, Germany), adhered to the European guidelines and to the guidelines of GV-SOLAS for animal welfare in science and were consistent with the ARRIVE guidelines.

Enzyme-linked immunosorbent assay (ELISA)

Progranulin protein expression in human serum and mouse plasma was analyzed with a progranulin enzyme immune assay kit (human: R&D Systems, #DPGRN0; mouse: Adipogen, #AG-45A-0019-YEK-KI01) according to the manufacturer's instructions. Samples were diluted 1:500 or 1:100, and 100 μ l of each sample was submitted to the assay. The absorbance was determined at 450 nm using a microplate reader (Tecan Infinite F200 Pro).

EAE model and bone marrow transplantation (BMX)

Mice on a C57BL/6 background (transgenic, knockout, and control mice) were immunized using Hooke Kit™ MOG35-55/CFA emulsion PTX (EK-2110, Hooke Labs, St Lawrence, MA), which contained 200 μ g of MOG 35–55 emulsified in 200 μ l of complete Freund's adjuvant (CFA). The mice received a subcutaneous (s.c.) injection of the emulsion at two sites followed by two intraperitoneal (i.p.) injections of 200 ng pertussis toxin (PTX) in phosphate buffered saline (PBS); the first PTX injection was administered 1–2 h after MOG35-55 injection, and the second one was administered 24 h after MOG35-55 injection.

SJL mice were immunized using Hooke Kit™ PLP139-151/CFA emulsion PTX (EK-2120), which contained 200 μ g of myelin

proteolipid protein (PLP) 139–151 in 200 μ l of CFA (Hooke Labs, US). Injections of the emulsion and PTX were performed as described above. Sample sizes for the EAE experiments were based on the recommendations of the Hooke labs (<https://hookelabs.com/>).

EAE scores and body weights were assessed daily by an observer blinded to the genotypes and treatments to evaluate the severity and extent of motor functional deficits. The scores were as follows: 0, normal motor functions; 0.5, distal paralysis of the tail; 1, complete tail paralysis; 1.5, mild paresis of one or both hind legs; 2, severe paresis of one or both hind legs; 2.5, complete paralysis of one hind leg; 3, complete paralysis of both hind legs; 3.5, complete paralysis of hind legs and paresis of one front leg.

For bone marrow transplantation (BMX), recipient mice received a 9.5 Gy cobalt 60 gamma irradiation followed by an intravenous injection of 6×10^6 bone marrow cells from the donor through the tail vein. Bone marrow cells were harvested from the tibia and femur of donor mice. One donor provided cells for two recipients. The immunization of the BMX recipients was performed with MOG35-55/CFA emulsion plus PTX (protocol C57BL/6J) as described above 3 weeks after BMX.

Blood was collected by puncture of the retrobulbar plexus or by cardiac puncture (final sample) into K^+ EDTA microtubes (EDTA K^+ Microvette Sarstedt) and centrifuged at 3000 rpm for 10 min and the plasma samples were stored in standard Eppendorf caps at -80°C until analysis. Samples for tissue analysis were obtained at the end of the score time course (28–35 days after immunization). Pieces of specific brain regions, the spinal cord, and peripheral tissues (spleen and lymph nodes) were rapidly dissected, snap frozen on dry ice and stored at -80°C .

In vivo imaging of immunization sites

In vivo imaging was performed with an IVIS Lumina Spectrum, which allows for the analysis of bioluminescence and near-infrared signals, and was analyzed with LivingImage software (PerkinElmer). Four, 8, 11, and 15 days after EAE immunization, 150 μ l of Xenolight RediJect Inflammation Probe (40 mg/ml; PerkinElmer), which recognizes myeloperoxidase activity, was injected intraperitoneally. Bioluminescence was captured 5, 10, and 15 min after injection in 9–10 animals per genotype to assess individual differences in Xenolight kinetics. During imaging, mice were kept under 1–1.5% isoflurane anesthesia. The IVIS settings were as follows: Epi-bioluminescence, emission filter open, excitation filter block, fstop = 1, binning = 8, focus B = 6.5 cm, exposure = 60 sec. The regions of interest (ROI) i.e., the injection sites, were identified by using the automatic detection tool in LivingImage. For each mouse, the two time points with the maximum total counts of bioluminescence in the ROIs were used to statistically analyze the genotype differences.

Immunofluorescence analysis of glial activation and immune cell infiltration

Mice were terminally anaesthetized with isoflurane and transcardially perfused with cold 0.9% NaCl followed by 4% paraformaldehyde (PFA) in 1x PBS for fixation. The spinal cord, brain, spleen, and lymph nodes were excised, postfixed in 4% PFA for 2 h, cryoprotected overnight in 20% sucrose at 4°C , embedded in tissue molds in cryomedium and cut on a cryotome (12 μ m). The slides were air-dried and stored at -80°C . After thawing, the slides were immersed and permeabilized in 1x PBS with 0.1% Triton-X-100 (PBST), blocked with 3% BSA in PBST, subsequently incubated overnight with a primary antibody in 1% BSA in PBST at 4°C , washed and incubated with a secondary fluorochrome (Alexa 488 or Cy3)-labeled antibody for 2 h at room temperature. The procedure was repeated for the other antibody pairs, and the slides were then incubated with 1 μ g/ml DAPI and mounted with Fluoromount (eBioscience). The general settings were optimized

for the respective primary antibodies, and the settings are listed in Supplementary Table 2.

Quantification of immunofluorescent images

Tiled images were captured and subsequently stitched to produce an image of the complete ventral horn of the spinal cord. Filter and acquisition parameters were set to assure comparability independent of genotype or treatment. Iba1+ and CD11b+ microglia/macrophages in the gray matter and white matter were quantified using the particle counter plugin of FIJI ImageJ. After each channel was converted to 8-bit, the background was subtracted, and the intensity threshold was set using the IJ IsoData algorithm in FIJI. For the particle counter, size inclusions were set to 5–575 μm^2 . The average sizes were 20 and 28 μm^2 for Iba1+ and CD11b+ particles, respectively. The number of particles and the area covered by immunoreactive cells relative to the total area (which was identical in all images) were used to assess the effects of genotype. Three or more nonoverlapping images from three mice were analyzed per group.

To assess the number of autophagosomes and lysosomes, the area and the perimeter of the respective particles per image were normalized to the area or perimeter of DAPI nuclei in the image. Hence, the percentages reflected the relative number of organelles within the cells. Three images were analyzed per group at different time points (0, 3, 6, and 24 h after 10 μ g/ml LPS stimulation).

Quantitative 3D colocalization of progranulin with HLA-DRA was assessed with FIJI ImageJ using Pearson's correlation coefficient and Manders' tM1 and tM2 coefficients above the autothresholds for channel 1 (HLA-DRA, red) and channel 2 (progranulin, red). The expression levels of HLA-DRA and progranulin upon stimulation with OVA were assessed by analyzing the area of immunofluorescence after the threshold was set according to Li's algorithm in FIJI. The fluorescence areas were normalized to the DAPI area to account for differences in the number of cells in each image.

Primary bone marrow-derived macrophages

Femurs and tibias were flushed with 1x PBS containing 0.5% penicillin/streptomycin, and the cells were collected by centrifugation (1500 rpm for 3 min at 4°C), subsequently resuspended and incubated for 10 min in 1 ml 1x erythrocyte lysis buffer. After centrifugation and resuspension, the cells were plated in RPMI 1640 containing 200 mM GlutaMax, 10% fetal calf serum (FCS), 1% penicillin/streptomycin, and 20 ng/ml macrophage colony stimulation factor (M-CSF) to initiate differentiation towards mature macrophages over 7 days. The cells were kept at 37°C in 5% CO_2 . BMDMs were used to assess phagocytosis, endocytosis, and antigen presentation.

Primary dendritic cells

Spleens were dissected, and DCs were isolated with the PanDC Negative Isolation Kit from MiltenyiBiotec (#130-100-875), which relies on the antibody-mediated removal of non-DC cells. After dissection, 500 μ l of the collagenase/dispase mixture was injected into the spleen, and the spleen was cut into small pieces and incubated in a petri dish for 30 min at 37°C . After mechanical disruption, which was performed by forcing the tissue through a nylon mesh with a pore size of 70 μ m (cell strainer, BD), the cells were washed with 1x PBS containing 0.5% FCS and 2 mM EDTA. An FcR-blocking reagent and a PanDC antibody cocktail were added and incubated for 10 min at 4°C . After the cells were washed and resuspended in 1x PBS, anti-biotin microbeads were added and incubated for 10 min at 4°C . A LS-MACS column was placed into the MACS separator and prepared by rinsing with 1x PBS. The cells were counted, and 10^7 cells were loaded onto the column. The cells were allowed to pass through, and the effluent containing the unlabeled DC-enriched cell fraction was collected.

The process was repeated, the cells were pooled and counted, and 1.5×10^6 cells per ml were seeded in 6-cm petri dishes.

Western blot analysis

Cultured BMDMs and DCs were harvested after 24 h of stimulation with vehicle, ovalbumin (EndoGrade, 50 $\mu\text{g/ml}$), LPS (0.1 $\mu\text{g/ml}$), or poly (I:C) (Sigma-Aldrich, 10 $\mu\text{g/ml}$). Whole cell protein extracts and tissue protein were prepared in radioimmunoprecipitation assay (RIPA) lysis buffer (Cell Signaling) containing a protease inhibitor cocktail (CompleteTM, Roche Diagnostics) and phenylmethylsulfonyl fluoride (PMSF, 10 $\mu\text{g/ml}$). The proteins were separated by 10–16% SDS-PAGE, transferred onto nitrocellulose membranes (Amersham Pharmacia) by electroblotting, incubated with the primary antibodies listed in Supplementary Table 2 and detected with secondary antibodies conjugated to IRDye 680 or 800 (1:10000; LI-COR Biosciences). Beta-actin or GAPDH were used as the loading control. Blocking was achieved with 5% skimmed milk in 0.1% Tween 20 in 1x PBS. All incubations were performed in Tris-buffered saline containing 0.5% Tween 20. The blots were visualized and analyzed on the Odyssey Infrared Imaging System (LI-COR Biosciences) and quantified with Image Studio Lite, and the ratio of each protein band versus the control band was used for quantitative assessment.

FACS analysis of surface marker proteins

Single-cell suspensions were prepared from the spleen, lymph nodes, and lumbar spinal cord. Tissues were rapidly dissected, treated with lysis buffer (DMEM/Accutase (PAA) (1:1), collagenase (3 mg/ml, Sigma-Aldrich), and DNase I (1 U/ml, Promega)) for 30 min at 37 °C, and mechanically disrupted by forcing the tissue through a nylon mesh with a pore size of 70 μm (cell strainer, BD). For FACS analysis of circulating cells, K+ EDTA blood was used. Blood samples and cell suspensions (100 μl) were mixed with 100 μl of HEPES buffer (20 mM HEPES) and 1 ml of erythrocyte lysis buffer for 10 min at room temperature and with CD16/32 blocking antibody (Fc γ RII/III receptor blocker, BD) for 15 min on ice. To stain the cell surface antigens, the cells were incubated for 20 min at room temperature in staining buffer with fluorochrome-labeled antibodies (Supplementary Table 2) and were then counted with a flow cytometer (BD FACS Canto II). FACS scans were analyzed with FlowJo 10. For all FACS assays, the antibody concentrations followed the recommendations of the manufacturers, and the controls were FITC, PE, or APC-conjugated rat IgG.

FACS analysis of intracellular cytokines

Single cell suspensions were prepared from the spleen by mechanical disruption by forcing the tissue through a nylon mesh with a pore size of 70 μm (cell strainer, BD), and the pellets were resuspended in PBS with 10% FCS. The cells were then stimulated with 50 ng/ml PMA and 500 ng/ml ionomycin for 8 h at 37 °C. After 2 h, 10 $\mu\text{g/ml}$ brefeldin A was added to disrupt Golgi-dependent secretion. The stimulated cells were then treated with erythrocyte lysis buffer for 10 min at room temperature and incubated overnight in fixation/permeabilization buffer (BD) at 18 °C. To stain the cell surface antigens and intracellular cytokines, the cells were incubated for 20 min at room temperature in permeabilization buffer with fluorochrome-labeled antibodies (Supplementary Table 2) and were then counted with a flow cytometer (BD FACS Canto II) and analyzed with FlowJo 10.

Phagocytosis assay

Phagocytosis was assessed with the Phagocytosis Assay Kit (Cayman Chemical, #500290). BMDMs were incubated for 2 h at 37 °C with FITC-labeled rabbit-IgG latex beads (diluted 1:200) or with FITC-labeled heat-killed *E. coli* particles (1:1000 dilution, Molecular Probes, #E-13231), washed with PBS and incubated for 20 min at room temperature in staining buffer with a CD11b antibody (Supplementary Table 2). The cells were then counted

with a flow cytometer (BD FACS Canto II), and the CD11b-FITC double-positive cells were gated and quantified with FlowJo 10.

Antigen presentation, uptake, and processing

C57BL/6J mice were injected with endotoxin-free ovalbumin (50 μg , i.p.) on days 0 and 3. The spleen was dissected on day 7, and DCs were isolated as described above. Cultured DCs were incubated with 50 $\mu\text{g/ml}$ DQ-ovalbumin (ThermoFisher) for 25 min at room temperature. After washing with 1x PBS, the cells were stained with CD11c-V450 for 20 min at room temperature and were then counted by FACS.

To analyze antigen presentation, DCs and OVA-specific CD4+ T-cells (OT cells) were isolated from the spleen of OVA-injected mice (see above). For OT isolation, single-cell suspensions were enriched via a CD4-negative isolation kit (Dyna) containing monoclonal antibodies against B220, CD11b, Ter-119, CD16/32, and CD8 following the protocol provided by the manufacturer. The cell preparations contained >90% of the desired cell population and were essentially free of CD11c^{high} cells, as determined by flow cytometry using antibodies specific for CD4, CD8, and CD11c. OT cells were stained with 1 μM CFSE-FITC (Molecular Probes) for 10 min at 37 °C. CFSE is a fluorescent dye that penetrates the cell membrane and is retained within cells. The analysis of proliferation was based on the decrease in fluorescence in dividing cells relative to a fluorescent bead standard. A total of 2×10^5 DCs were incubated for 1 h with 100 $\mu\text{g/ml}$ EndoGrade OVA at 37 °C in complete medium. The cells were then washed 3x and resuspended in complete medium containing 2×10^5 CFSE-labeled OT cells. The proliferation of T-cells was analyzed by flow cytometry after 2.5 days of coculture with DCs. To analyze T-cell proliferation independent of APCs, OTs were isolated as described above and labeled with CFSE. The cells were cultured in 96-well plates in complete medium with or without 50 $\mu\text{g/ml}$ PMA and were analyzed after 2.5 days. The cells were stained with a CD4 antibody (Supplementary Table 2) for 20 min and counted with a flow cytometer (BD FACS Canto II), and CD4-FITC double-positive cells gated and quantified with FlowJo 10.

Statistics

The data are presented as scatter plots showing the mean \pm standard deviation or as box plots, in which the box is the interquartile range and the whiskers show the minimum and maximum. The time course data of EAE scores are the mean \pm SEM. The data were analyzed with SPSS 23 and GraphPad Prism 6.0 or 7.0. Differences in serum concentrations between the groups were analyzed using analysis of variance (ANOVA), two-sided unpaired *t*-test or the Mann–Whitney U test according to the data structure and distribution. Normal distribution was assessed with the D'Agostino–Pearson normality test. Further analyses were performed by χ^2 statistics. Time courses were analyzed by repeated-measures analysis of variance (2-way ANOVA) using time and genotype as factors. In the case of significance by ANOVA, the groups were compared using *t*-tests, and the *P*-value was adjusted according to the procedures of Dunnett (versus one control group) or Sidak. The Friedmann test was used to compare nonparametric EAE scores. In addition, the AUCs of the EAE-score vs. time curves were calculated using the trapezoidal method, and AUCs were subsequently analyzed by the Mann–Whitney U test (2 groups) or Kruskal Wallis test (>2 groups). The alpha level was set at 0.05 for all comparisons, and the adjusted values are reported. The quantification of the immunofluorescence data is explained above.

ACKNOWLEDGEMENTS

The study was supported by the Deutsche Forschungsgemeinschaft (CRC1080, A3 to IT and MS; CRC1039 to IT) and the research funding program "Landesoffensive zur Entwicklung wissenschaftlich-ökonomischer Exzellenz" (LOEWE) of the State of

Hessen, Research Center for Translational Medicine and Pharmacology, TMP. We thank Sabine Wicker for collecting blood samples from human controls and Dominique Thomas for the analysis of lipid levels in serum samples.

AUTHOR CONTRIBUTIONS

KS, VV, and AWS performed the experiments and analyzed the data. KS performed all of the in vivo and ex vivo EAE experiments. VV assessed colocalization in the cell lines. RB collected human samples and clinical data. MS contributed colocalization expertise. IT initiated the study, analyzed clinical, FACS and image data, made the figures, and created and revised the manuscript. All authors contributed to and approved the final version of the manuscript.

ADDITIONAL INFORMATION

The online version of this article (<https://doi.org/10.1038/s41423-019-0274-5>) contains supplementary material.

Competing interests: The authors declare no competing interests.

REFERENCES

1. Cruts, M. et al. Null mutations in progranulin cause ubiquitin-positive frontotemporal dementia linked to chromosome 17q21. *Nature* **442**, 920–924 (2006).
2. Baker, M. et al. Mutations in progranulin cause tau-negative frontotemporal dementia linked to chromosome 17. *Nature* **442**, 916–919 (2006).
3. Gotz, J. K. et al. Common pathobiochemical hallmarks of progranulin-associated frontotemporal lobar degeneration and neuronal ceroid lipofuscinosis. *Acta Neuropathol.* **127**, 845–860 (2014).
4. Mackenzie, I. R. et al. The neuropathology of frontotemporal lobar degeneration caused by mutations in the progranulin gene. *Brain* **129**, 3081–3090 (2006).
5. Schafer, M. K. E. & Tegeder, I. NG2/CSPG4 and progranulin in the posttraumatic glial scar. *Matrix Biol.* **68–69**, 571–588 (2018).
6. Naphade, S. B. et al. Progranulin expression is upregulated after spinal contusion in mice. *Acta Neuropathol.* **119**, 123–133 (2010).
7. Tanaka, Y., Matsuwaki, T., Yamanouchi, K. & Nishihara, M. Increased lysosomal biogenesis in activated microglia and exacerbated neuronal damage after traumatic brain injury in progranulin-deficient mice. *Neuroscience* **250**, 8–19 (2013).
8. Yin, F. et al. Exaggerated inflammation, impaired host defense, and neuropathology in progranulin-deficient mice. *J. Exp. Med.* **207**, 117–128 (2010).
9. Ahmed, Z. et al. Accelerated lipofuscinosis and ubiquitination in granulin knockout mice suggest a role for progranulin in successful aging. *Am. J. Pathol.* **177**, 311–324 (2010).
10. Filiano, A. J. et al. Dissociation of frontotemporal dementia-related deficits and neuroinflammation in progranulin haploinsufficient mice. *J. Neurosci.* **33**, 5352–5361 (2013).
11. Lui, H. et al. Progranulin deficiency promotes circuit-specific synaptic pruning by microglia via complement activation. *Cell* **165**, 921–935 (2016).
12. Altmann, C. et al. Progranulin promotes peripheral nerve regeneration and reinnervation: role of notch signaling. *Mol. Neurodegener.* **11**, 69 (2016).
13. Tang, W. et al. The growth factor progranulin binds to TNF receptors and is therapeutic against inflammatory arthritis in mice. *Science* **332**, 478–484 (2011).
14. Neill, T. et al. EphA2 is a functional receptor for the growth factor progranulin. *J. Cell Biol.* **215**, 687–703 (2016).
15. Altmann, C. et al. Progranulin overexpression in sensory neurons attenuates neuropathic pain in mice: Role of autophagy. *Neurobiol. Dis.* **96**, 294–311 (2016).
16. Tanaka, Y., Chambers, J. K., Matsuwaki, T., Yamanouchi, K. & Nishihara, M. Possible involvement of lysosomal dysfunction in pathological changes of the brain in aged progranulin-deficient mice. *Acta Neuropathol. Commun.* **2**, 78 (2014).
17. Chang, M. C. et al. Progranulin deficiency causes impairment of autophagy and TDP-43 accumulation. *J. Exp. Med.* **214**, 2611–2628 (2017).
18. Jian, J. et al. Association Between Progranulin and Gaucher Disease. *EBioMedicine* **11**, 127–137 (2016).
19. He, Z., Ong, C. H., Halper, J. & Bateman, A. Progranulin is a mediator of the wound response. *Nat. Med.* **9**, 225–229 (2003).
20. Zhou, M. et al. Progranulin protects against renal ischemia/reperfusion injury in mice. *Kidney Int* **87**, 918–929 (2015).
21. He, Z. & Bateman, A. Progranulin gene expression regulates epithelial cell growth and promotes tumor growth in vivo. *Cancer Res.* **59**, 3222–3229 (1999).
22. Fu, W. et al. Foxo4- and Stat3-dependent IL-10 production by progranulin in regulatory T cells restrains inflammatory arthritis. *FASEB J.* **31**, 1354–1367 (2017).
23. Wei, F., Zhang, Y., Zhao, W., Yu, X. & Liu, C. J. Progranulin facilitates conversion and function of regulatory T cells under inflammatory conditions. *PLoS One* **9**, e112110 (2014).

24. Suh, H. S., Lo, Y., Choi, N., Letendre, S. & Lee, S. C. Evidence of the innate antiviral and neuroprotective properties of progranulin. *PLoS One* **9**, e98184 (2014). eCollection 2014.
25. Park, B. et al. Granulin is a soluble cofactor for toll-like receptor 9 signaling. *Immunity* **34**, 505–513 (2011).
26. Holler, C. J., Taylor, G., Deng, Q. & Kukar, T. Intracellular proteolysis of progranulin generates stable, lysosomal granules that are haploinsufficient in patients with frontotemporal dementia caused by GRN mutations. *eNeuro* **4**, eN-NWR-0100-17 (2017). eCollection Jul–Aug.
27. Zhou, X. et al. Prosaposin facilitates sortilin-independent lysosomal trafficking of progranulin. *J. Cell Biol.* **210**, 991–1002 (2015).
28. Fujita, E. et al. Two endoplasmic reticulum-associated degradation (ERAD) systems for the novel variant of the mutant dysferlin: ubiquitin/proteasome ERAD(I) and autophagy/lysosome ERAD(II). *Hum. Mol. Genet* **16**, 618–629 (2007).
29. Beel, S. et al. Progranulin functions as a cathepsin D chaperone to stimulate axonal outgrowth in vivo. *Hum. Mol. Genet* **26**, 2850–2863 (2017).
30. Zhou, D. et al. Lamp-2a facilitates MHC class II presentation of cytoplasmic antigens. *Immunity* **22**, 571–581 (2005).
31. Kondylis, V. et al. Endosome-mediated autophagy: an unconventional MHC-driven autophagic pathway operational in dendritic cells. *Autophagy* **9**, 861–880 (2013).
32. Schmid, D., Pypaert, M. & Munz, C. Antigen-loading compartments for major histocompatibility complex class II molecules continuously receive input from autophagosomes. *Immunity* **26**, 79–92 (2007).
33. Bhattacharya, A., Parillon, X., Zeng, S., Han, S. & Eissa, N. T. Deficiency of autophagy in dendritic cells protects against experimental autoimmune encephalomyelitis. *J. Biol. Chem.* **289**, 26525–26532 (2014).
34. Weindel, C. G. et al. B cell autophagy mediates TLR7-dependent autoimmunity and inflammation. *Autophagy* **11**, 1010–1024 (2015).
35. Finch, N. et al. Plasma progranulin levels predict progranulin mutation status in frontotemporal dementia patients and asymptomatic family members. *Brain* **132**, 583–591 (2009).
36. Huang, K. et al. Progranulin is preferentially expressed in patients with psoriasis vulgaris and protects mice from psoriasis-like skin inflammation. *Immunology* **145**, 279–287 (2015).
37. Tanaka, A. et al. Serum progranulin levels are elevated in patients with systemic lupus erythematosus, reflecting disease activity. *Arthritis Res Ther.* **14**, R244 (2012).
38. Lotsch, J. et al. Machine-learned data structures of lipid marker serum concentrations in multiple sclerosis patients differ from those in healthy subjects. *Int J. Mol. Sci.* **18**, E1217 (2017).
39. Schiffmann, S. et al. Ceramide synthase 6 plays a critical role in the development of experimental autoimmune encephalomyelitis. *J. Immunol.* **188**, 5723–5733 (2012).
40. Pawlitzki, M. et al. CSF-progranulin and neurofilament light chain levels in patients with radiologically isolated syndrome-sign of inflammation. *Front Neurol.* **9**, 1075 (2018).
41. Kimura, A. et al. Increased cerebrospinal fluid progranulin correlates with interleukin-6 in the acute phase of neuromyelitis optica spectrum disorder. *J. Neuroimmunol.* **305**, 175–181 (2017).
42. Hardt, S. et al. Loss of synaptic zinc transport in progranulin deficient mice may contribute to progranulin-associated psychopathology and chronic pain. *Biochim Biophys. Acta* **1863**, 2727–2745 (2017).
43. Kao, A. W. et al. A neurodegenerative disease mutation that accelerates the clearance of apoptotic cells. *Proc. Natl Acad. Sci. USA* **108**, 4441–4446 (2011).
44. Phillips, J. A., Rubin, E. J. & Perrimon, N. Drosophila RNAi screen reveals CD36 family member required for mycobacterial infection. *Science* **309**, 1251–1253 (2005).
45. Hawkes, M. et al. CD36 deficiency attenuates experimental mycobacterial infection. *BMC Infect. Dis.* **10**, 299 (2010).
46. Bieghs, V. et al. Internalization of modified lipids by CD36 and SR-A leads to hepatic inflammation and lysosomal cholesterol storage in Kupffer cells. *PLoS ONE* **7**, e34378 (2012).
47. Sanjurjo, L. et al. The human CD5L/AIM-CD36 axis: a novel autophagy inducer in macrophages that modulates inflammatory responses. *Autophagy* **11**, 487–502 (2015).
48. Tanaka, Y. et al. Progranulin regulates lysosomal function and biogenesis through acidification of lysosomes. *Hum. Mol. Genet* **26**, 969–988 (2017).
49. Tegeder, I. Yeast-2-Hybrid data file showing progranulin interactions in human fetal brain and bone marrow libraries. *Data Brief.* **9**, 1060–1062 (2016).
50. Suarez-Calvet, M. et al. CSF progranulin increases in the course of Alzheimer's disease and is associated with sTREM2, neurodegeneration and cognitive decline. *EMBO Mol. Med* **10**, e9712 (2018).
51. Li, H. et al. Circulating PGRN is significantly associated with systemic insulin sensitivity and autophagic activity in metabolic syndrome. *Endocrinology* **155**, 3493–3507 (2014).
52. Martens, L. H. et al. Progranulin deficiency promotes neuroinflammation and neuron loss following toxin-induced injury. *J. Clin. Investig.* **122**, 3955–3959 (2012).

53. Miller, Z. A. et al. TDP-43 frontotemporal lobar degeneration and autoimmune disease. *J. Neurol. Neurosurg. Psychiatry* **84**, 956–962 (2013).
54. Thurner, L. et al. The molecular basis for development of proinflammatory autoantibodies to progranulin. *J. Autoimmun.* **61**, 17–28 (2015).
55. Menzel, L. et al. Progranulin protects against exaggerated axonal injury and astrogliosis following traumatic brain injury. *Glia* **65**, 278–292 (2017).
56. Keller, C. W. et al. ATG-dependent phagocytosis in dendritic cells drives myelin-specific CD4(+) T cell pathogenicity during CNS inflammation. *Proc. Natl Acad. Sci. USA* **114**, E11228–E11237 (2017).
57. Stoeckle, C. et al. Cathepsin S dominates autoantigen processing in human thymic dendritic cells. *J. Autoimmun.* **38**, 332–343 (2012).
58. Zhou, S. et al. Autophagy is involved in the pathogenesis of experimental autoimmune neuritis in rats. *Neuroreport* **27**, 337–344 (2016).
59. Seto, S., Tsujimura, K., Horii, T. & Koide, Y. Autophagy adaptor protein p62/SQSTM1 and autophagy-related gene Atg5 mediate autophagosome formation in response to *Mycobacterium tuberculosis* infection in dendritic cells. *PLoS One* **8**, e86017 (2013).
60. Egashira, Y. et al. The growth factor progranulin attenuates neuronal injury induced by cerebral ischemia-reperfusion through the suppression of neutrophil recruitment. *J. Neuroinflamm.* **10**, 105 (2013).
61. Chen, X. et al. Progranulin does not bind tumor necrosis factor (TNF) receptors and is not a direct regulator of TNF-dependent signaling or bioactivity in immune or neuronal cells. *J. Neurosci.* **33**, 9202–9213 (2013).
62. Reuter, E. et al. Role of sortilin in models of autoimmune neuroinflammation. *J. Immunol.* **195**, 5762–5769 (2015).
63. Gass, J. et al. Progranulin regulates neuronal outgrowth independent of Sortilin. *Mol. Neurodegener.* **7**, 33 (2012).
64. Hu, F. et al. Sortilin-mediated endocytosis determines levels of the frontotemporal dementia protein, progranulin. *Neuron* **68**, 654–667 (2010).
65. Chen, Y. et al. Progranulin associates with hexosaminidase A and ameliorates GM2 ganglioside accumulation and lysosomal storage in Tay-Sachs disease. *J. Mol. Med.* **96**, 1359–1373 (2018).
66. Cai, X. et al. Expression and polymorphisms of lysosome-associated protein transmembrane 5 (LAPTM5) in patients with systemic lupus erythematosus in a Chinese population. *Biochem. Genet.* **53**, 200–210 (2015).
67. Vercellino, M. et al. Progranulin expression in brain tissue and cerebrospinal fluid levels in multiple sclerosis. *Mult. Scler.* **17**, 1194–1201 (2011).
68. Schmitz, K. et al. Dysregulation of lysophosphatidic acids in multiple sclerosis and autoimmune encephalomyelitis. *Acta Neuropathol. Commun.* **5**, 42 (2017).